Chapter 11: The context of cratering: Mare Orientale, Mare Nectaris, Moscoviense Basin, and Vredefort Structure

Abstract

Understanding how the various cratering structures interact allow us to interpret the geomorphic features seen with them. Studying the cratering structure of Mare Orientale, Mare Nectaris, and Moscoviense Basin by comparing Crustal Thickness, Free Air Anomaly, and topographic views allows us to discern a tentative cross section view and how the various parts are structurally related to each other and their origin. These processes are then applied to South Africa and the cratering context of the Vredefort Dome Structure and a possible scenario is developed to explain the goldfields found under that structure. The interaction of these larger crater with the mantle is emphasized as a source of the Moho on the Earth and the lunar discontinuity on the Moon.

Keywords: Mare Orientale, Mare Nectaris, Moscoviense Basin, Vredefort Dome Structure

Introduction

In the last chapters we explored a few examples of craters on both the moon and earth and observed how their structure involves ghost craters, both circular and straight Concentric Global Ring Structures (CGRS), and differing energy input of the shock/compression wave and the release/expansion wave. Now we are ready to see how these various energy sources working together formed the visible structures.

Mare Orientale

Viewing Mare Orientale in the Topography map (Figure 11.1), the Free Air Gravity map, and the Crustal Thickness map, two rings become significant. The smaller half circle of yellow in Crustal Thickness is the same as in Free Air Gravity showing the mascon (red in Free Air Gravity) corresponds to the area of central uplift (blue in Crustal Thickness). I will refer to this ring as the Open-ring, and postulate it represents the size of hole punched in the lunar disconformity (LD, which corresponds to the Moho on the earth). The mascon corresponds to the area of thinnest crust and allows the density of the local mantle to effect the relatively shallow gravity reading. As was shown in Chapter 10B, this would correspond to mountain uplift within the Open-ring on earth and their correspondence to CGRS on the moon. Some of these CGRS effecting Mare Orientale are indicated between arrows in Figure 11.1. The most visible evidence for these CGRS are release valleys.

The larger second half circle, yellow in Free Air Gravity and black in Crustal Thickness, I will recognize as the original crater rim (OCR)-ring. The reverse colored dotted half circle in both figures better represent the present cratering rim, but the solid linear better represents the point of highest shock/compression wave representation. It is reasonable that the shock wave would have a peak and taper off to either side (Figure 1.3), and the cratering rim break would occur to the side where the compression peak transitioned into the release valley, part way down the energy and physical slope. This confirms that the crustal structures of cratering are a temperature and energy response, not simply a blasting limit as Shoemaker (1974) and NASA (Keifer, 2003) suggest (Figure 8.3). The rim was pushed up by the shock/compression wave and the valley, in this case the entire crater, is filled by the release/expansion wave's adiabatic response sediments.

Mare Orientale has a very visible ray halo completely surrounding the OCR ring in Crustal Thickness. The pairs of arrows in Topography, Free Air Gravity, and Red Relief show these "rays" do not originate in the OCR, but cross the open and inner rings and are among the CGRSs responsible for the mascon.

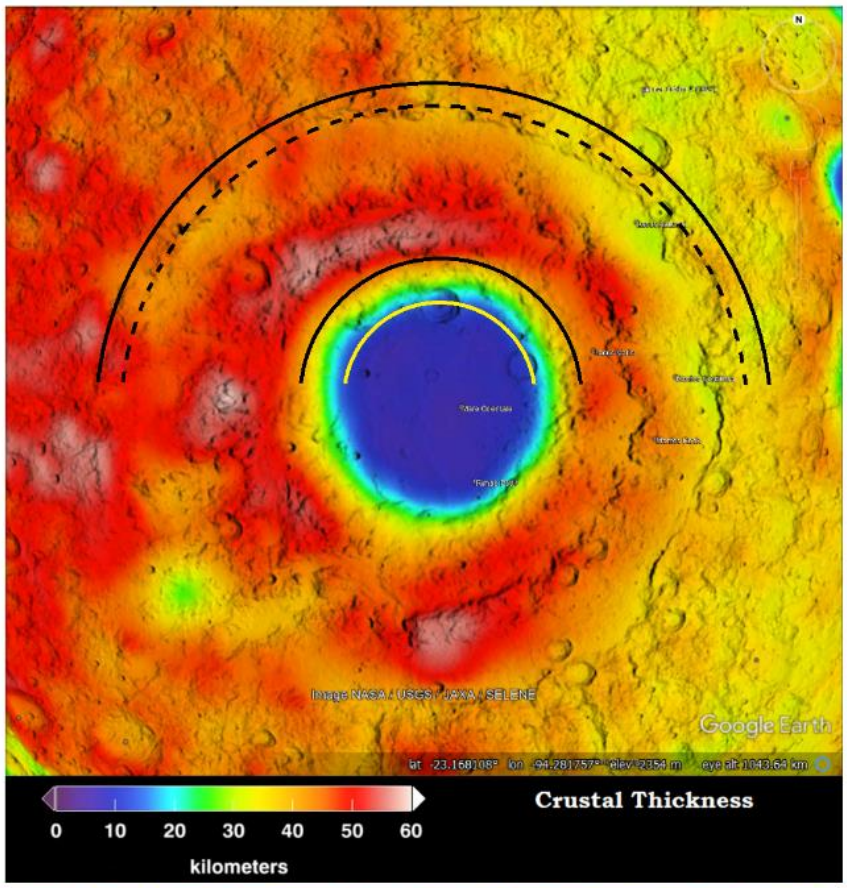

Figure 11.1: Views of Mare Orientale gathered from NASA and JAXA missions to the Moon. Pairs of arrows show linears of CGRS visible in each data set. (Image credit: Free Air Gravity, Crustal Thickness, and Topography, NASA; Red Relief, Chiba 2019)

Figure 11.2A shows the surface contours and depth of crust (Crustal Thickness map) as it possibly related originally to the uplift at the center of the crater. Figure 11.2B shows a bullseye pattern of alternating high and low gravity readings laid on Mare Orientale like the one developed in Figure 10.18-19 for the Green River Crater. The cross section shows the five rings of Hartmann and Kuiper (1962). They determined the diameter from rectified photos from earth telescopes: Inner Ring 320 km, 2nd Ring 480 km, 3rd Ring 620 km, Eichstadt Ring 930 km, and Rocca Ring 1300 km. The “Rocca Ring” corresponds to the “2nd Ring” in Figures 11.2 and 3.

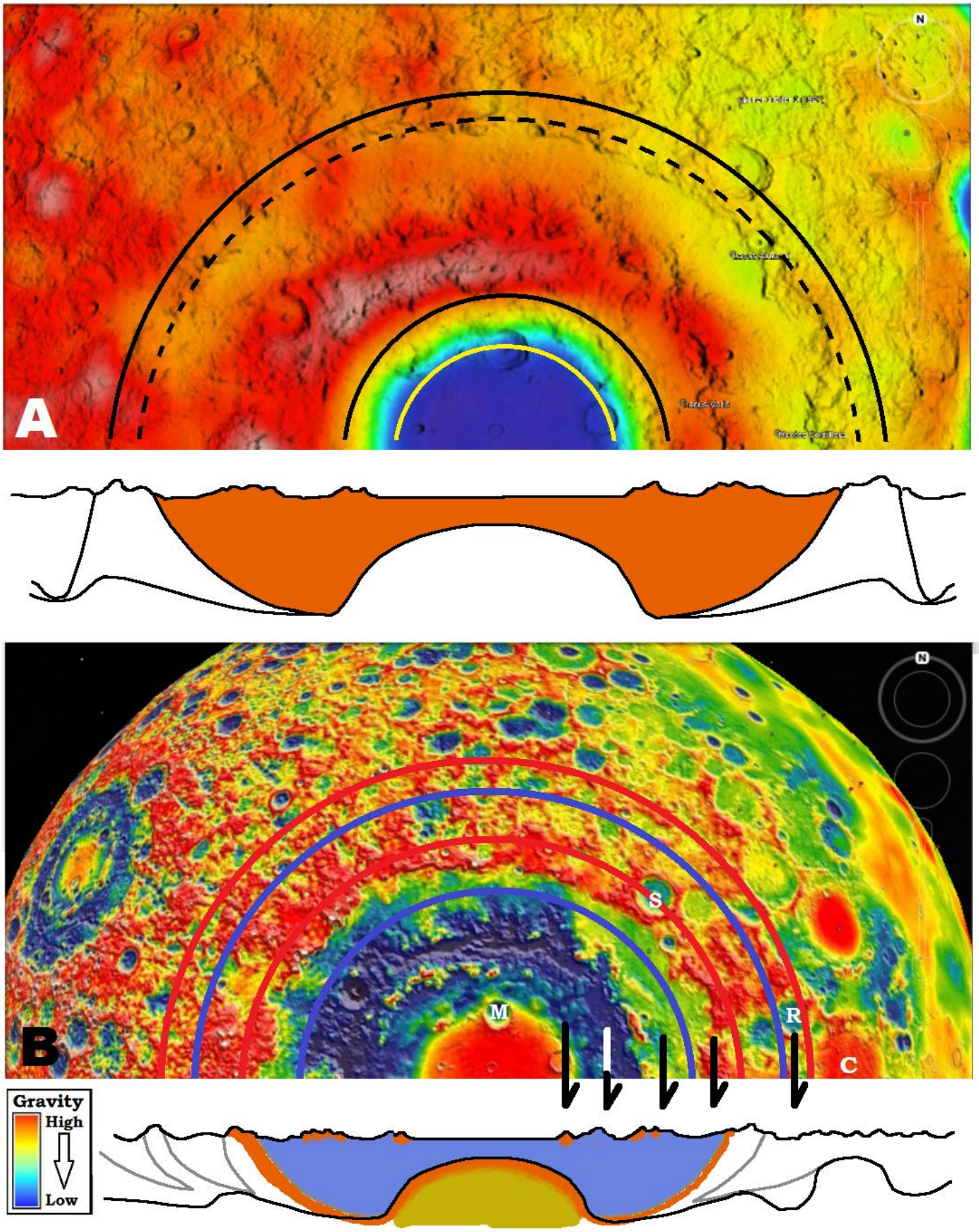

Figure 11.2: (A) Crustal Thickness, (B) GRAIL with proposed cross sections by the author. Five black arrows represent the rings Hartmann and Kuiper (1962) measured from rectified photographs. For scale, the Inner-ring and mantle uplift is ~300 km diameter. Maunder (M), Schlüter (S), Rocca (R), and Crüger (C) craters are labeled.

As Mare Orientale is a large compound crater, look at some simple craters in its vicinity. Within the central mascon, Figure 11.2B, the Maunder (M) Crater (~54 km diameter) leaves a low gravity circle that overpowers the high gravity reading of the mascon. Schlüter (S) (~180 km diameter) and Rocca (R) craters (~84 km diameter) also have blue, low gravity reading floors, with only the Schlüter having a small point of higher gravity occurring in its center. This leads to the conclusion, except for the mascon changing the center of some larger craters, the natural state for inside the OCR is for it to be low gravity except for the central uplift, showing it filled with low gravity fallback.

If the crater is filled with low density --the rim is high density material--, there are recurring glimpses of low gravity outside the rim. These recurring low gravity rings may have only been partial lows because they are easily overcome with the high gravity rings of subsequent smaller craters while low gravity fill of the central crater did not react the same way. The cross section below Figure 11.2B shows an interpretation of the underlying pattern of high and low gravity structure derived from Free Air Gravity map and determination of possible original structural arrangement outside the OCR before the superimposing of energy signature from additional craters.

Figure 11.3 shows a more detailed representation of this same generalized cross section of Mare Orientale. The Inner ring is included at its position above the edge of the center uplift. The interrupting mascon occurring under the small Crüger crater is included but has lost most of its indication of rings. That mascon and the crater which originally accompanied that impact, certainly occurred prior to Mare Orientale and was largely obliterated by the energy signature, not the ejecta, of the later crater. This shows an interaction of energy waves and heat in the overlapping impacts and suggest the two impacts were not separated by a large amount of time that allowed the energy from the Crüger crater to dissipate.

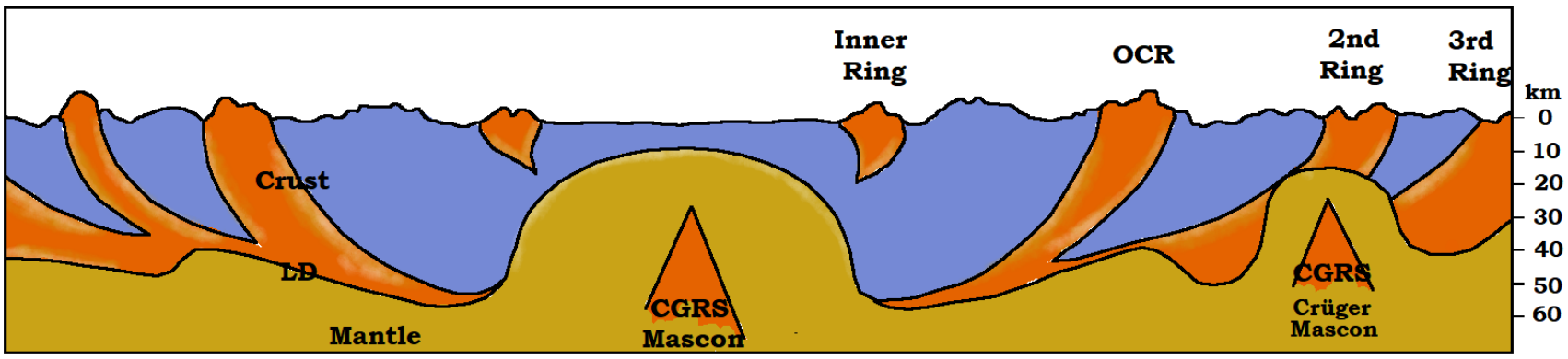

Figure 11.3: A speculative generalized cross section through Mare Orientale based on Figure 11.2B, accounting for the location of high (red) and low (blue) gravity readings and the elevation of the central area which lifted in response to rebound piercing the bowl of high density material produced by the shock wave. The Lunar Discontinuity (LD), equivalent to the Moho on earth, defines the edge of compressed material, which separates the crust from the mantle.

Mare Nectaris

Comparing Figure 11.4 Crustal Thickness and Free Air Gravity shows that both Mare Nectaris and Sinus Asperitatis each have separate filled bowl shaped depressions and a separate ring structures surrounding them. This identifies each as separate impact craters but Mare Nectaris's impactor arrived last and overwhelmed the energy expression of the earlier Asperitatic impactor. The blue interior of the Theophilus (~99 km diameter), Catharina (~99 km diameter), and Piccolomini (~88 km diameter) craters again supports the conclusion that a crater without a mascon naturally has a low gravity crater fill.

Hartmann and Kuiper (1962) recognized three rings around Mare Nectaris: Inner ring 400 km diameter, Catharina ring (weak) 600 km diameter, Altai ring at 840 km diameter. As the Altai Scarp provides the limit of bowl shape in Crustal Thickness, it is recognize as the OCR ring for the crater.

Piccolomini Crater and Mare Nectaris

Comparing the yellow ridge of the Altai Scarp (AS), Figure 11.4, ring on Topography map, the ridges are most prominent in the regions with clear yellow arcs within them in the Crustal Thickness map. The crust is thinner within the release wave valley annulus, just inside the Altai Scarp, showing the release wave did not push the Moho down as far as the shock/compression wave, thus a slightly lower gravity reading. The red mascons in Free Air Gravity and their correlation with blue areas of thinned crust in Crustal Thickness identify additional craters which have little or no indication in Topography and Red Relief supporting the occurrence of many large ghost craters in the vicinity.

The less distinct occurrence of Fracastorius crater (F) (120 km diameter) at the southern edge of Mare Nectaris, while larger than Theophilus crater (~99 km diameter) or Maunder crater in Mare Orientale, fails to show the same drop in the mascon's high gravity reading. This difference may reflect the Fracastorius impactor arrived closer to the time of the Mare Nectaris impactor so the smaller shock-release waves were swallowed into the larger energy pattern.

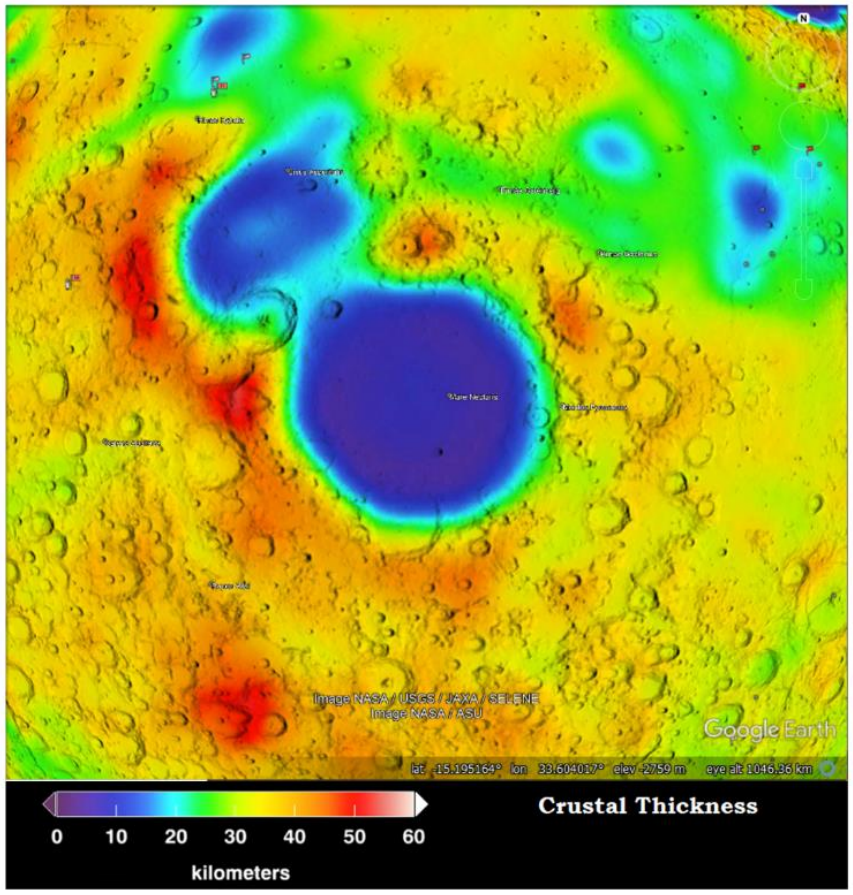

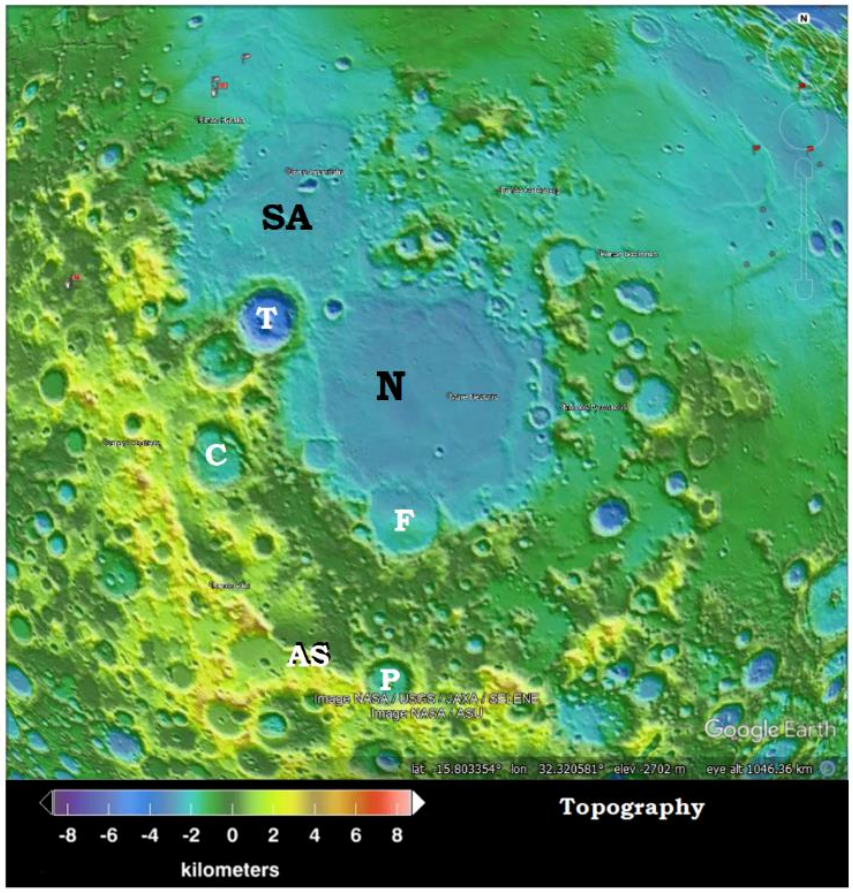

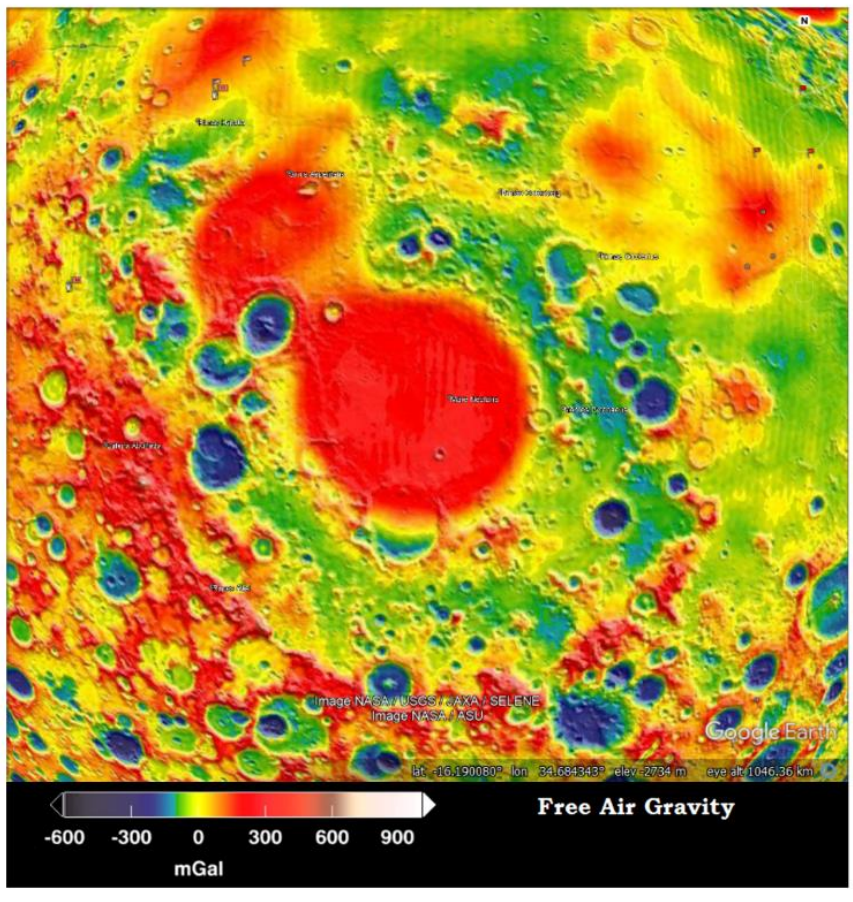

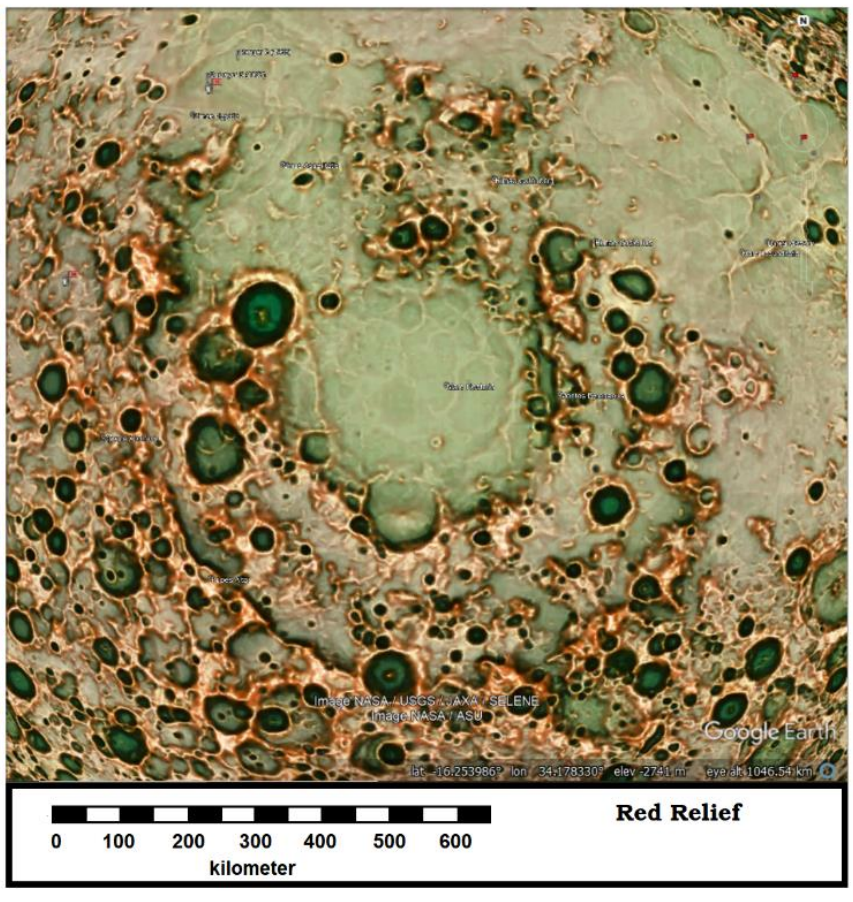

Figure 11.4: Four views of Mare Nectaris (N), Open ring = 325 km. Fracastorius (F) 120 km diameter. T = Theophilus crater, C = Catharina crater, P = Piccolomini crater, SA = Sinus Asperitatis, AS = Altai Scarp. (Image credit: Red Relief, JAXA (Chiba 2019), other three, NASA.)

Using four different craters as centers, some of the CGRS are mapped around Mare Nectaris. In Figure 11.5, the white circled numbers show intersect paths within the Mare Nectaris crater, and Black circled numbers label more obvious linears outside the crater. Anderson Crater made numerous ridges and valleys through the area, as do the Mare Orientale and Grimaldi craters. Using the center of Sinus Iridum, on the north edge of Mare Imbrium, the perpendicular linear of dense crust at the northwest end of Sinus Asperatatis and another linear (red) of denser crust beyond that.

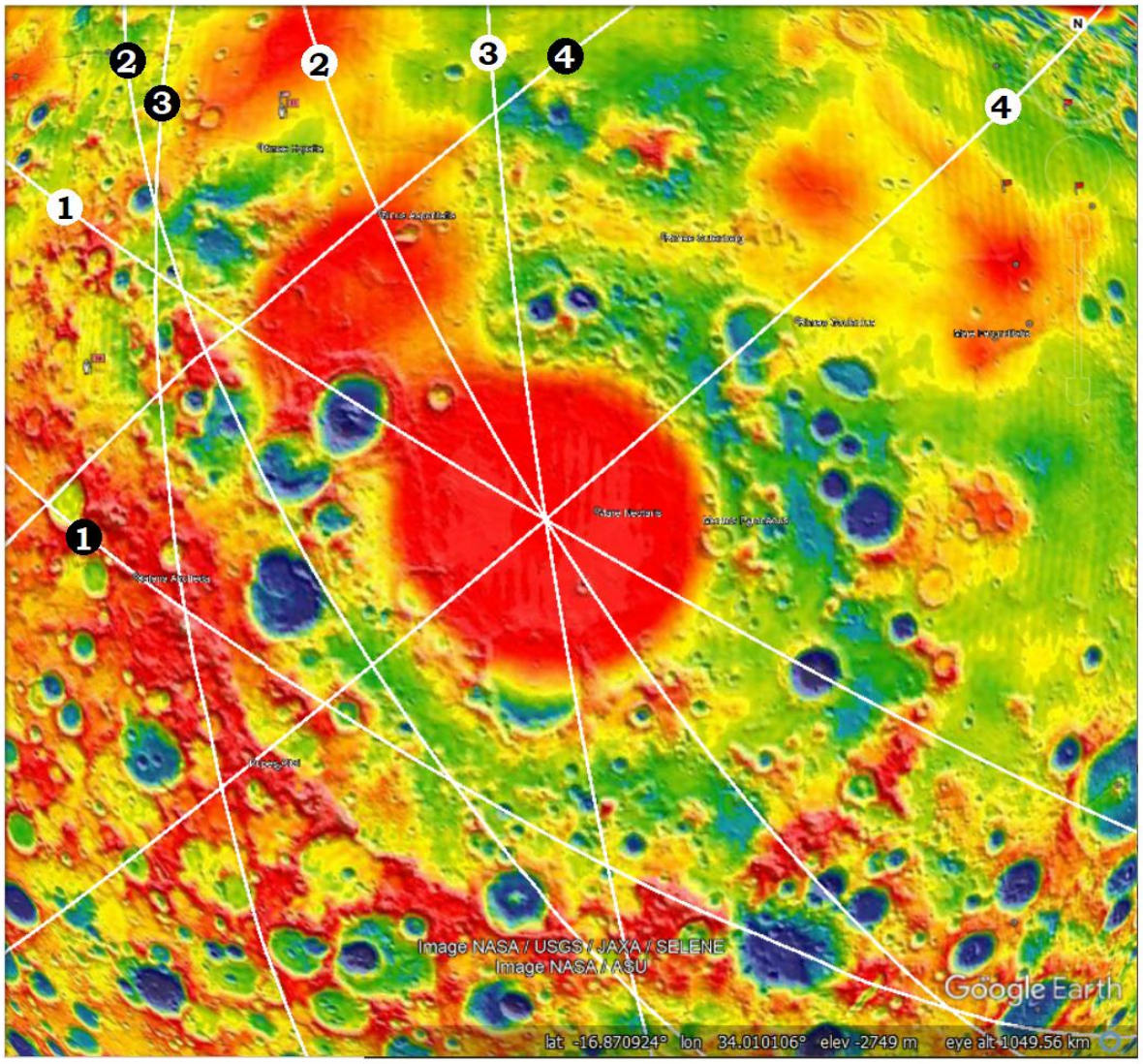

Figure 11.5: CGRS from 1= Anderson Crater, 2=Mare Orientale, 3 = Grimaldi Crater, 4= Iridum Basin, under Sinus Iridum, north of Mare Imbrium. Linears numbered in Black shows their relationship to Sinus Asperitatis and Mare Nectaris's mascons. Numbers in white show more visible linear's path.

Based on the Free Air Gravity map, Figure 11.6 is a generalized cross section of the Mare Nectaris and Sinus Asperitatis craters showing the comparative density and proposed sectioned shape of their rings as originally formed.

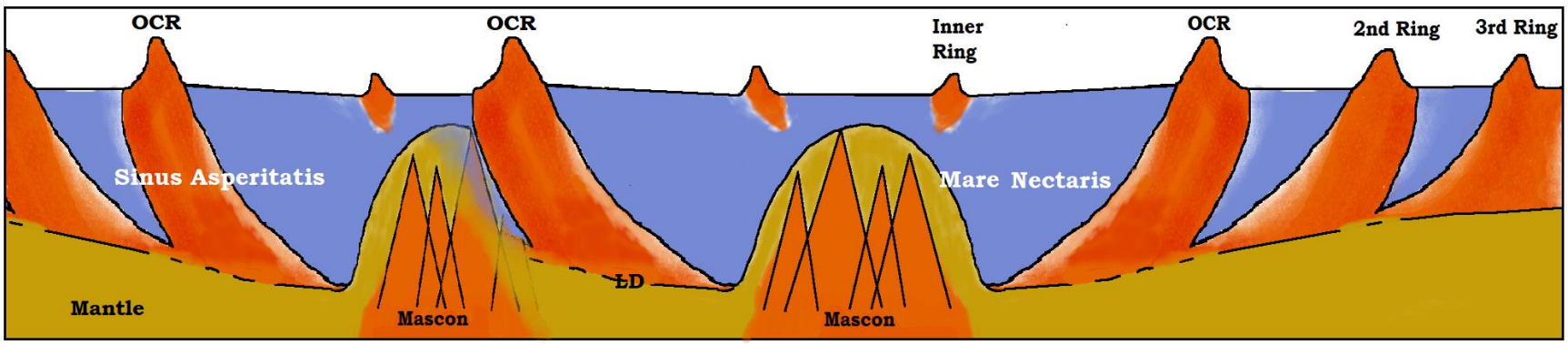

Figure 11.6: Generalized cross section of Mare Nectaris and Sinus Asperitatis showing the placement of the interaction of their rings.

Moscoviense basin

A major crater on the farside of the moon is the Moscoviense crater. As a casual view of the crater reveals, all rings do not relate to the same center. Thaisen et al (2011) recognized a maximum of three centers, and considered if the elongated shape might relate to an oblique impact? They also consider the probability of multiple impacts that merge into a single ring system. Ishihara et al (2011) also considered the oblique impact possibility. They option for two impacts where the later impact struck inside the first ring structure overlaying its pattern only over a portion of the earlier ring structure.

Comparing a ring around the mascon in Free Air Gravity with the blue area of thin crust in Crustal Thickness, Figure 11.7, shows the second crater's Open-ring. The small black ring defines the Open-ring for crater one, and provides a center for the outer pair of black half circles that define the outer edge of the red bowl shape in Crustal Thickness. I will put the OCR Ring again between these lines.

The Free Air Gravity shows CGRS centered in Mare Humboldtianum (white arrows) make very pronounced linears through the center of Moscoviense and both sides of the center within the low gravity ring, they push it even lower (darker blue). This shows that the release wave of the CRS are aligned there, leaving the shock wave between them to form the mascon in the center of the crater.

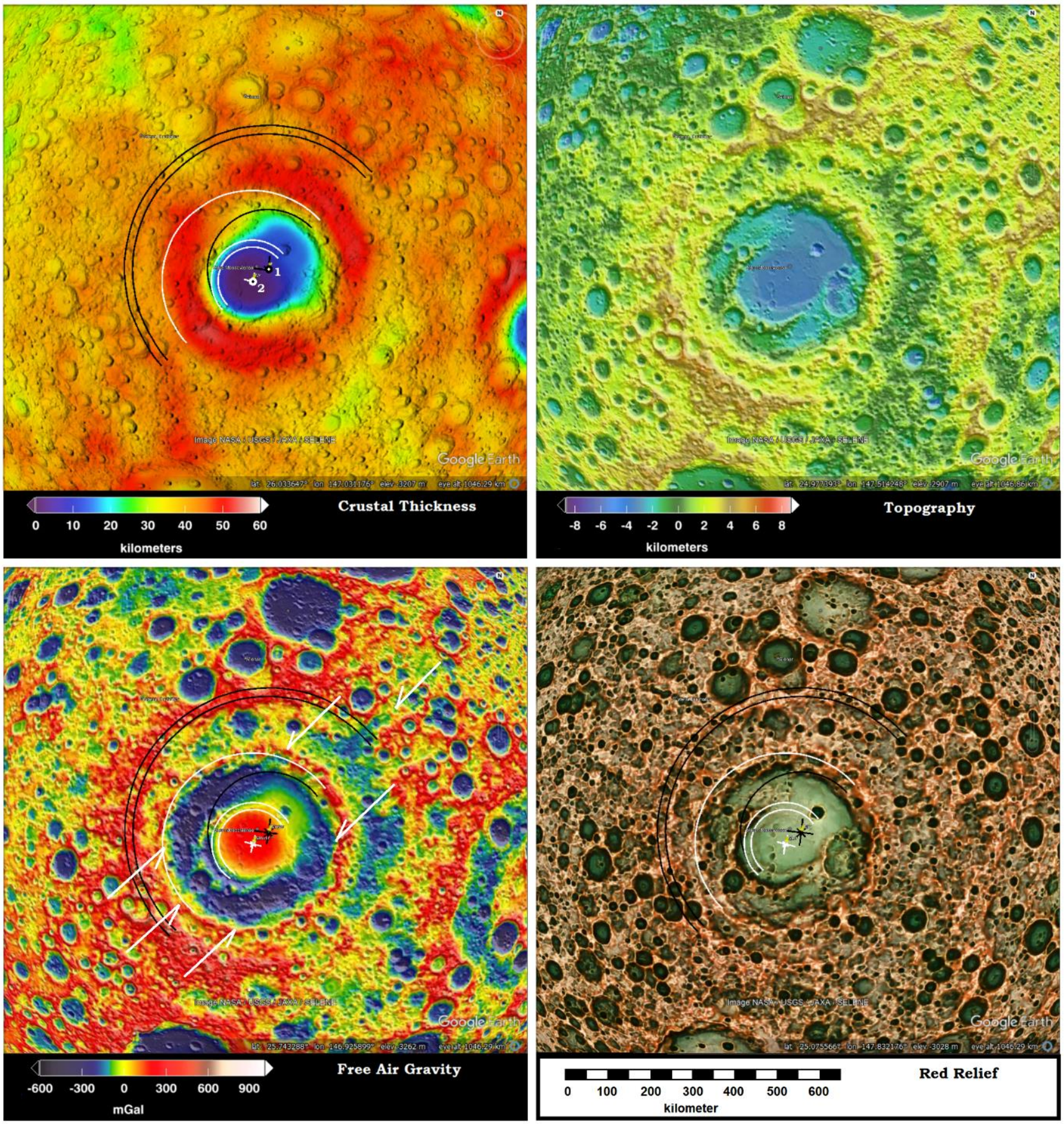

Figure 11.7: Four maps of Moscoviense Basin with Open-ring ~170 km. (Image credit: Same as Figure 11.4.)

Figure 11.8Aa recognizes the two bowl shapes, are not only nested but off set to the west for crater two. Ishihara et al (2011) provides a cross section using SELENA satellite data, Figure 11.8Ab. It shows the thinnest crust on the moon lies in the center of the second crater.

As the cratering rings move outwards, the second crater adds to the total energy in the crust, showing more red (high density) to the west of the Moscoviense Basin where its high density rings would overlay the low density rings of crater one. I would propose impactor one landed several minutes ahead of impactor two because the crater bowl seems to have formed before impactor two

arrived. Yet, impactor two arrived before significant energy dissipation had taken place, so that both heat/energy signatures were combined into a single pattern.

The gravity image, Figure 11.8B, shows a clear bullseye pattern for three pairs of wave expressions outwards.

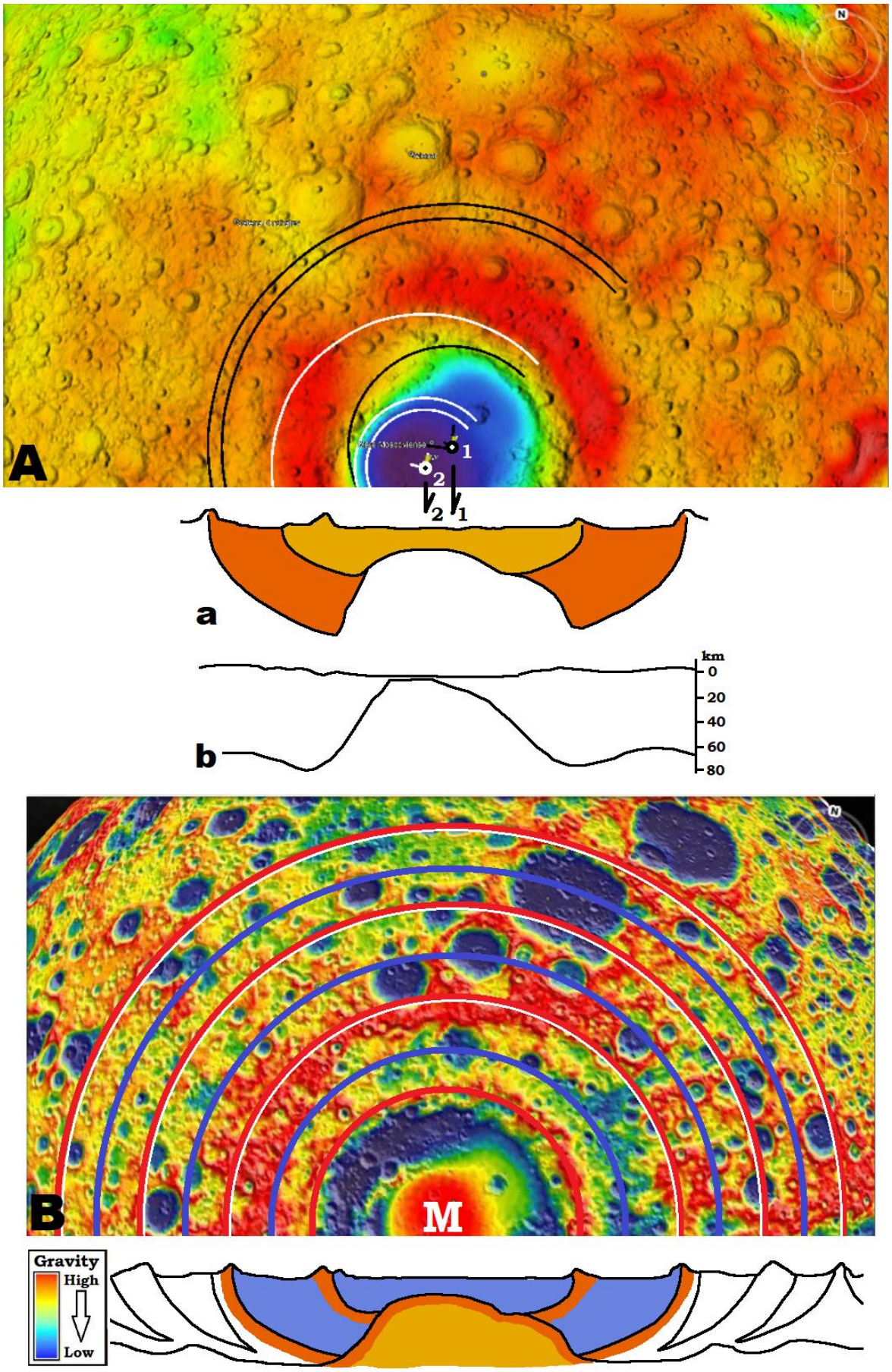

Figure 11.8: (A) Cross section of Crater bowl with half images same as Figure 11.2. Crustal Thickness map (B) Bullseye pattern detail of Figure 10.9

Figure 11.9 shows recurrent expression of shock/compression wave's beyond the stacked bowls of the original craters forming alternating high and low bands in a generalized cross section.

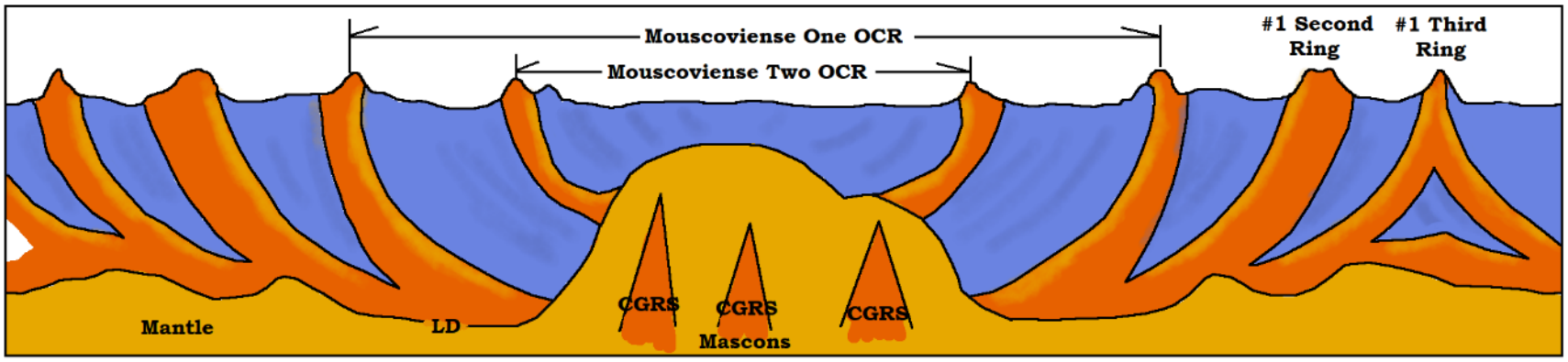

Figure 11.9: Mouscoviense basin showing the stacked bowls of the crater, then the second and third ring for the first impactor. CGRS are passing through mascon center

Using the cross sections developed here, Figure 11.10 provides a model of how the rings of high and low gravity develop, including the inner/open ring, a first, second and third ring.

(A) An impactor struck the moon's crust with the mantle directly underneath. When an impact hole was produced, the shock wave's compression formed the first lunar discontinuity (LD) into the mantle.

(B) Once the LD formed, it acted as a cohesive to hold the base of the hole together as it started to uplift.

(C) The uplift continued upwards into a jetting event carrying part of the early low density, adiabatic sediments on its upward moving surface.

(D) The adiabatic sediments continued to condense and settle on the jetting surface and base of crater. As the jetting column collapsed, the shock-release wave pair moved outside the crater rim with a compression-expansion wave producing a toroid of alternating high and low gravity readings forming outwards.

(E) If a portion of the compressed base of crater is carried sufficiently upwards it is stranded on the top surface of the low gravity fallback.

(F) The inner ring of high gravity material floating on low gravity sediments is the result.

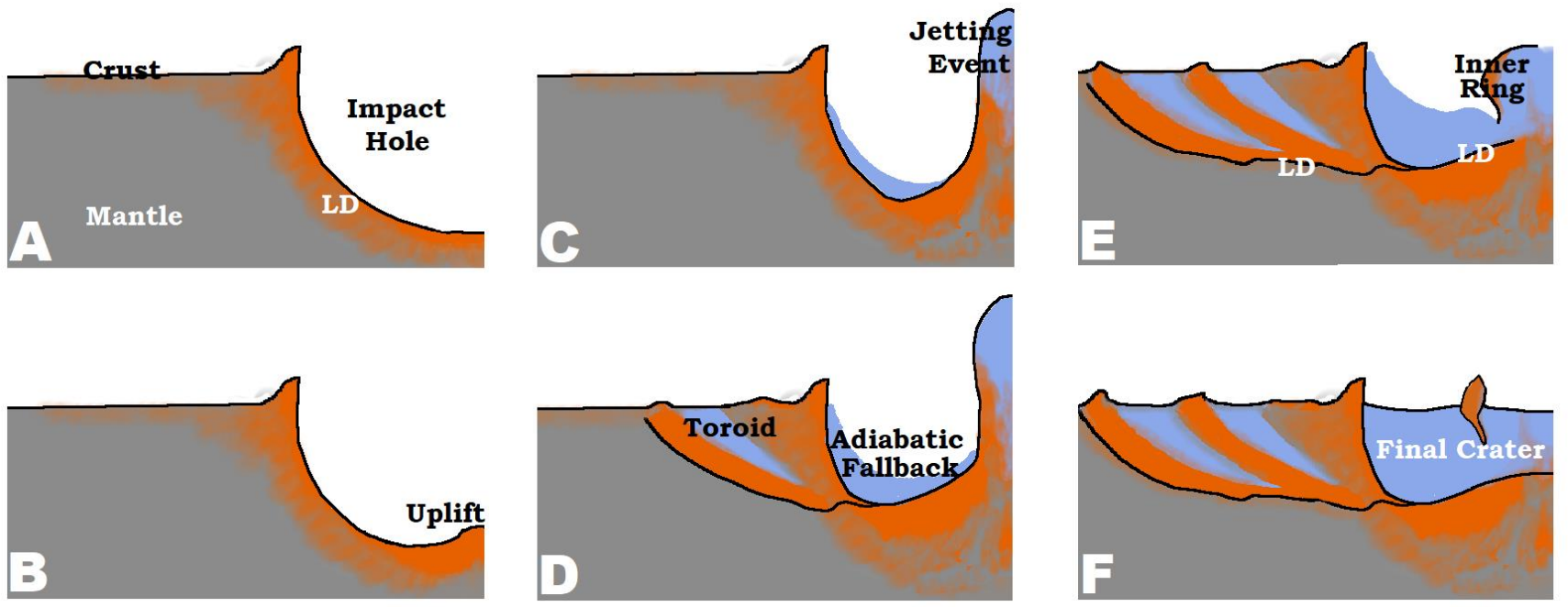

Figure 11.10: Sequence of events to form the inner ring from the jetting event.

Vredefort Structure and its cratering context

The understanding of the Vredefort structure and its inherited goldfield is depended on understand the regional cratering history of the greater southern Africa region, Figure 11.11. The plate tectonic explanation for the region involves several separate island arcs converging in orogenies over a few billion years. The cratering history is no less complex but it provides a lasting record of where and how these eight cratering events took place over a relatively short period of time. While this short discussion cannot be exhaustive, it will suggest a general connections between these craters, found in topography and gravity maps, and the geomorphic structures shaped by them.

The first structure leaving a record is the Indlovu crater followed rapidly by the Mabule crater and the Chobe and the Bulaway craters. While both of these last two's cratering centers are well north of the area considered, Chobe crater is centers between Zambia,

Botswana, and Namibia, and Bulaway crater centers in Zimbabwe (Table 1), both of their craters extend well into South Africa (Figure 11.11). Chobe and Bulaway craters left enough of their energy in the crust that the Mabule Crater has the gap in its expression across its northern border (Chapter 2) from them.

The Mabule crater is the defining structure for southern Africa's continental margins, but by contrast, Indlovu crater left its eastern third in the Indian Ocean, so it probably predates the Mabule crater's defining of the continent edges. Does the Mabule crater fulfill the statement in Psalm 104: 5, "Who [Jehovah] laid the foundations of the earth that it should not be moved for ever" [KJV]? Did the Mabule crater form this portion of the "foundation"? It appears to have done so.

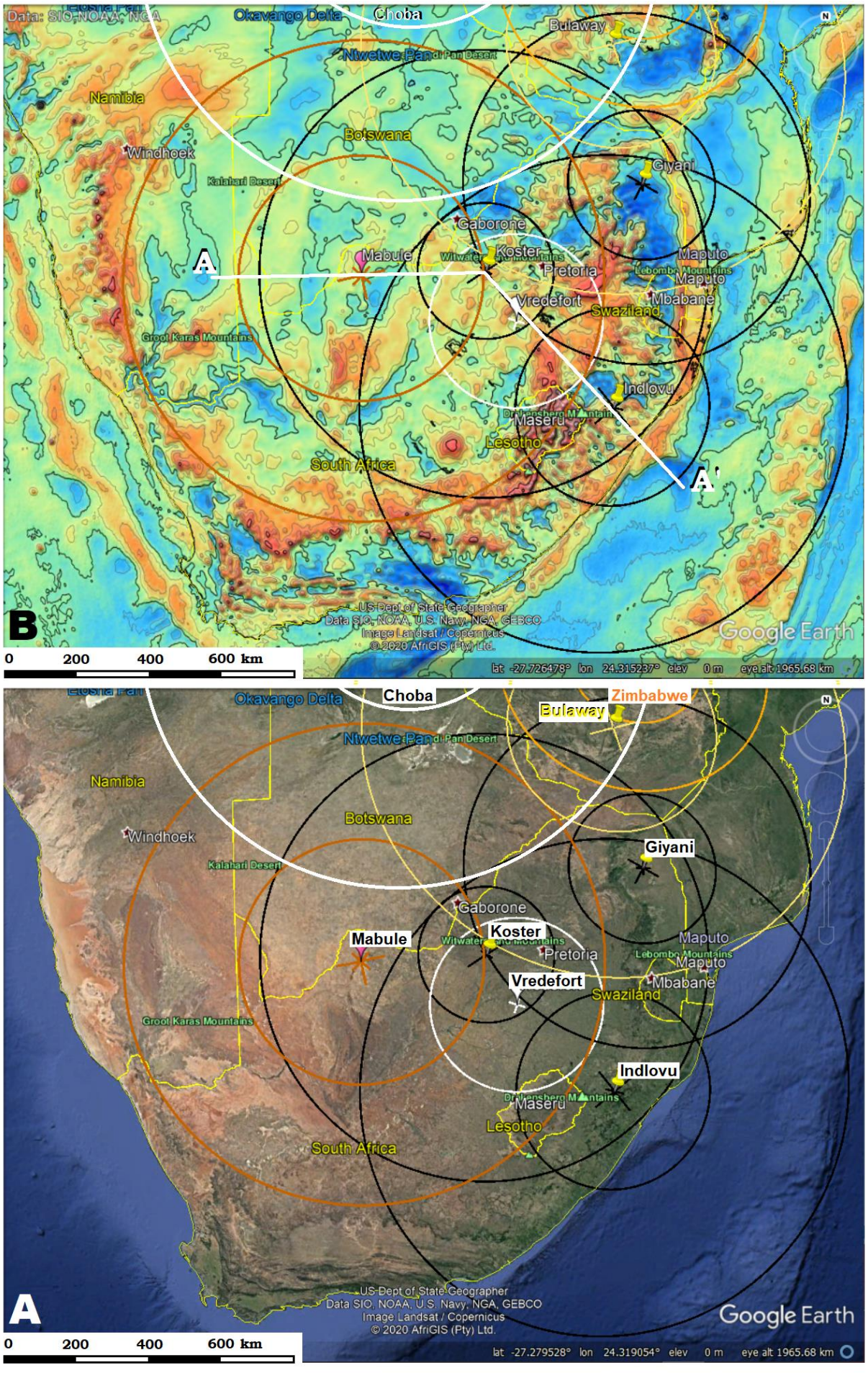

Figure 11.11: Some of the larger craters identified by their circular lineaments in southern Africa.

Geomorphic features of South Africa

The Limpopo Metamorphic Belt complex terrain (Figure 11.12A) was formed where the Indlovu crater nearly met the earlier Bulaway craters. The Bulaway crater would have heated the rock into a plastic state, so that the Indlovu buckled it up on edge to form the Northern Marginal Zone. An additional CGRS forms a lineament across to the Mozambique Channel, but all this was heavily modified by later cratering and other CGRS arriving in the near time scale. The Indlovu crater also overlapped the Mabule crater where the Witwatersrand strata would later occur and both of them contributed to the energy and events which would draw the carbon, gold and diamonds from deep in the mantle.

The slightly later Koster impactor (Figure 11.12B) excavated the crater for the Witwatersrand Basin and the ejecta that included amygdaloidal mafic metavolcanics (Jackson 1994) of the Dominion Group. This fallback continued to form the West Rand "reef" where the adiabatic process (Chapter 10) deposited the gold nuggets suddenly condensed in the air, not eroded from the ground, as well as the carbon droplets and nodules and diamonds which makes up the Central Rand's conglomerate. While the literature tries to find the connection between the Vredefort Structure, above the goldfields and the gold, Tucker (2016) admits the discussion is very much still open, and I suggest a cratering origin needs to be considered but for the Koster not the Vredefort's Crater. The abundant granitic and feldspar rich boulders and cobbles of Altermann and Lenhardt (2012) speak for power in such an ejection process, and the inclusion of komatiite requires an atmosphere of extreme heat and pressure which cratering provides. (Ejecta is used here to refer to breccia ejection by the cratering process, by contrast to the usual eruption of liquids associated with large igneous provinces.)

These deposits are found along paths of CGRS, rather than "limiting river beds." As episodic waves came from the crater center, the fractures would open and close and spew forth new deposits amongst the depositing ejecta from the Mabule impactor suggesting both craters were forming and secondarily reacting at the same time.

Abundant among the gold flakes and nuggets are seams and streamers of "fly speck" carbon (Tucker et al 2012). Upon examination of this carbon it is found to be in the form of almost microscopic solidified droplets which after leaching the quartz matrix off shows a structure of columns streaming to the back from a face that is melted in flight. There is no explanation for this unique ubiquitous structure in a low temperature environment. The structural integrity of the diamond crystals would also suggest formation in air, not cleaving out of a solidified matrix.

The sediments that formed the Ventersdorp and Transvaal Supergroups were deposited on the conglomerate by direct condensation from the remaining cloud of condensates according to the sequence of Africanis et al (2002) from magma vapors.

Slightly later the impactor that would form the Bushvelt Complex (Figure 11.12C) and the several that would define the limits of the Kaapvaal Craton (Figure 11.13) would arrive within hours or days of the Vredefort crater and each leave their arced print on the topography as ghost craters.

Since Bushveld Complex overlies the Giyani Inner ring, it likely originated after the Giyani impact, which would account for its inner ring sculpting the south edge of the complex. The complex fills the triangle of overlap between the Mabule, Zimbabwe and Indlovu, each contributing to the heat bank, provided the needed heat to fractionate the layered intrusive igneous deposit. Bushveld Complex's origin is given as in-situ differentiation or successive magma batches. Another alternative is successive layers of condensates precipitated by an impact crater. I propose the crater is represented by the dimensions of red granite (Figure 11.12C, yellow ring).

If successive cratering is continuing to add heat, what temperature are we talking about? After several separate cratering events raised the temperature of the rock past 1650-1720^{o} C, the melting point of forms of quartz toward 2800^{o} C, the melting point of Coesite, all within a few days, latent heat affecting the visibility of later smaller craters whose heat signature became totally lost in the hot bed of the existing rock, and subsequent producing the mass of ghost craters that are found. The Vredefort crater is one such "ghost" crater. The impactor struck the sedimentary layers of the Kaapvaal Craton and immediately pierced it raising the granulite and amphibolite of the central dome (Figure 8.20). The outward progressing shockwave gained its first expression at the Vredefort's collar, which is possibly equivalent to an inner ring, and producing concentric fractures and shock expressions until it got to its OCR and formed the limits of the basin from underneath the surface strata.

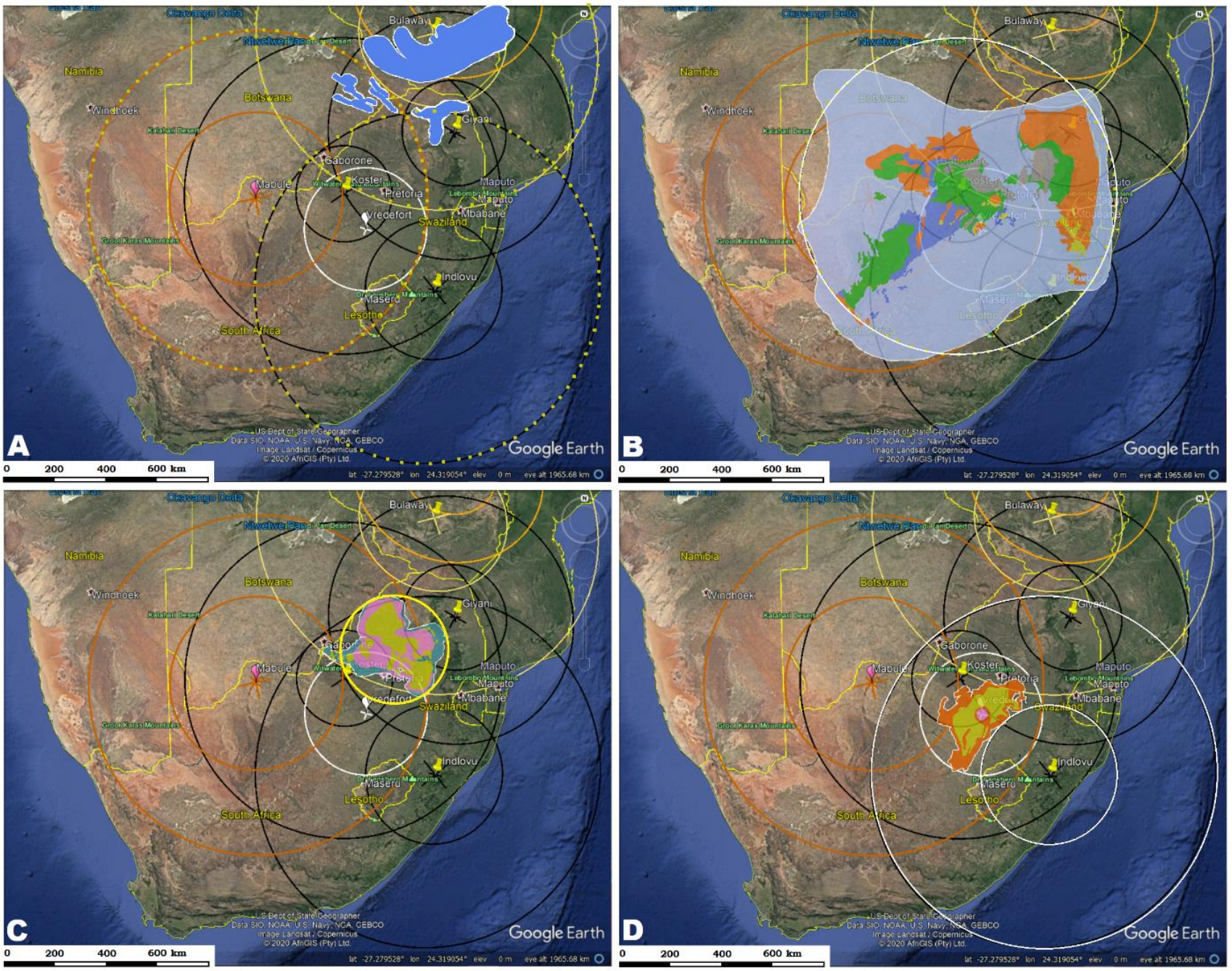

Figure 11.12: (A) The Limpopo Belt Complex. (B) The Kaapvaal Craton defined by the Koster Crater. (C) The crater shaped Bushveld Complex. (D) Vredefort Structure within the overlap from the Indlovu and Mabule Craters.

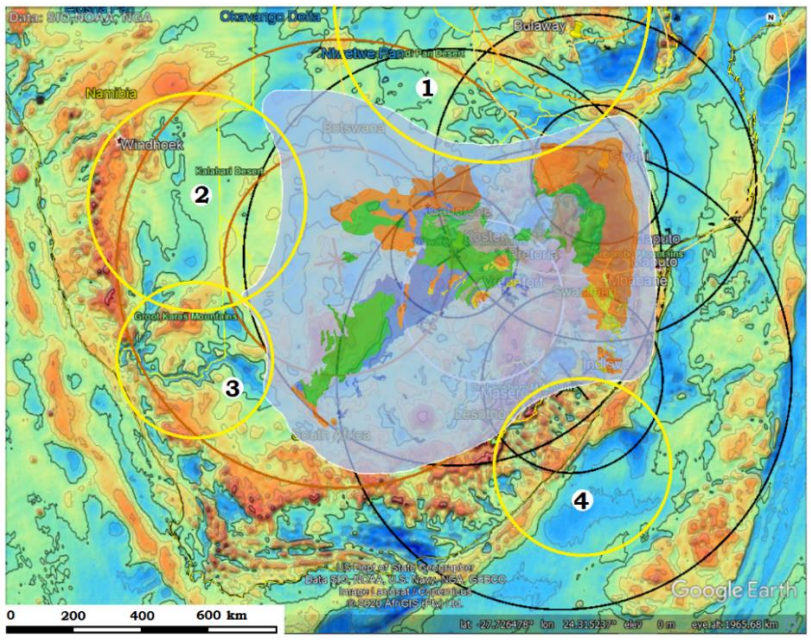

Figure 11.13: The Kaapvaal Basin, pale blue, showing 4 of the unnamed smaller impactors whose craters shaped the edge of the basin, along with the Koster crater that produced its sediments.

Name	Latitude	Longitude	Dia. Inner	Dia. OCR
Chobe	-17.634	24.463	860	1465
Bulaway	-20.16	29.99	585	1350
Indlovu	-29.07	30.24	520	1350
Mabule	-26.03	23.35	660	1300
Giyani	-23.65	30.81	400	960
Koster	-25.88	26.68	350	1200
Zimbabwe	-18.26	30.61	384	788
Vredefort	-27.06	27.51		485

Table 11.1: Basic statistics on the eight circular lineaments, which I will refer to as craters, in southern Africa.

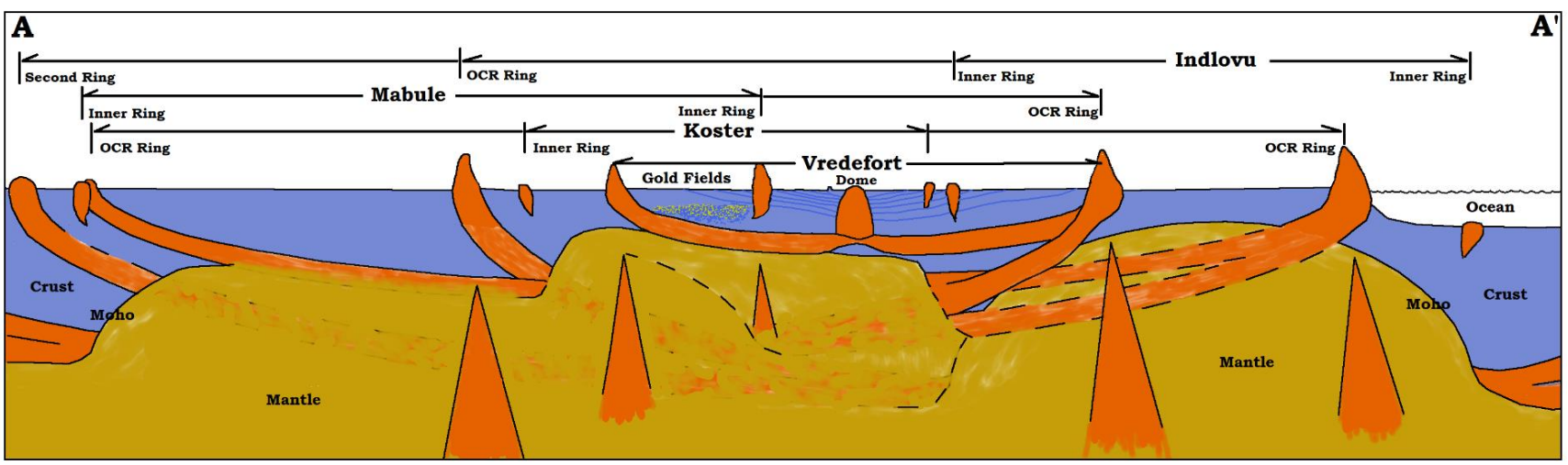

Figure 11.14: A generalized cross section of South Africa showing a partial pattern of high and low gravity layers and rings with a projected elevation of the Moho based on the pattern of gravity layers. Path as shown in white line of Figure 11.11B.

Tomographic images are attained by measuring *P*-wave resistivity, producing a view of the deep planet that is generally banded. The banding measured the comparative speed of through that portion of substrate. Blue is generally faster and red is slower. High density and temperature would generally speed up the transmission of energy and low density and temperature would generally slowdown transmission. This means colors will be approximately reversed from density, but the patterns would be retained. I would suggest one interpretation of the pattern as a series of overlapping craters. The most surprising attribute to this image is the depth to which cratering appears to have penetrated, and supports the assertion that cratering can account for much of the discontinuities down through the lithosphere and asthenosphere.

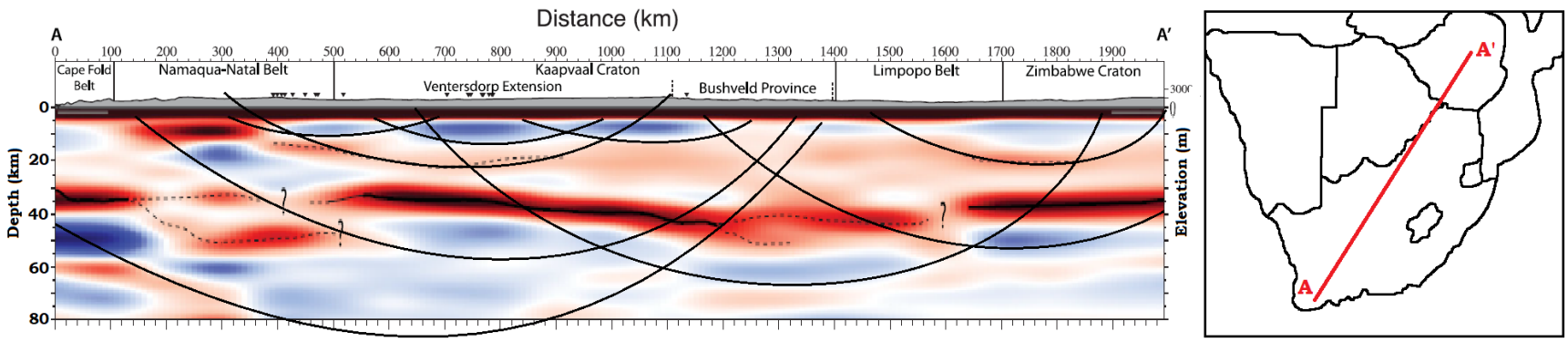

Figure 11.15: Tomographic section through Southern Africa (Image modified from Delph and Porter, 2015.)

Conclusions

What we see today, including the South African gold deposits, are not the result of a single cratering event, but requires a careful exploration of contributing cratering events and the energy response from each. There is a lot of theory to cratering which is unfamiliar to the average geologist, but if the goal is to understand the process enough that additional goldfields can be discovered, this process needs to continue to be explored

Each reader will have to decide for themselves whether this matching up of formations and ring structures can be attributed to coincidence without exceeding their credulity. Let me encourage the reader, if you have gotten this far, there is an abundance of information on these formations on the web. Look up a little for yourselves and see if the information has been dealt with honestly. No matter what model for origins we use, none of us were there to witness the events. All we can depend on is an honest dealing with all of the evidence we can find, and making the most sense out of it that we can. Be encourage to look for yourselves. The trust can

always stand up to close, closer, and closest scrutiny. Never fear to ask questions, if you are going to be diligent to search out an answer and willing to believe the answer you find.

References

Africano, F., G. Van Rompaey, A. Bernard, and F. Le Guern. 2002. Deposition of trace elements from high temperature gases of Satsuma-Iwojima volcano. *Earth Planets Space* 54:275-286.

Altermann. W. and N. Lenhardt. 2012. The Volcano-sedimentary succession of the Archean Sodium Group. Ventersdorp Supergroup. South Africa: Volcanology, facies and geochemistry, *Precambrian Research* 214–215: 60-81.

Chiba, T. 2019. Red relief image map of moon: Asia Air Survey, National Astronomical Observatory of Japan, Geospatial Information Authority of Japan, Japan Aerospace Exploration Agency, https://www.gsi.go.jp/chirijoho/chirijoho41026.html, accessed 9/13/19.

Delph, J.R. and R.C. Porter. 2015. Crustal structure beneath southern Africa: insight into how tectonic events affect the Mohorovičić discontinuity, *Geophysical Journal International* 200:254-264.

GRAIL Map https://svs.gsfc.nasa.gov/4014 accessed 4/25/2020.

Hartmann, W.K. and G.P. Kuiper. 1962. No. 12 Concentric structures surrounding lunar basins, *Communications of the Lunar and Planetary Laboratories* 1:51-66.

Ishihara, Y., T. Morota, R. Nakamura, S. Goossens, and S. Sasaki. 2011. Anomalous Moscoviense basin: Single oblique impact or double impact origin? *Geophysical Research Letters* 38, L03201.

Jackson, M.C. 1994. Geochemistry and metamorphic petrology of Dominion Group metavolcanics in the Vredefortt area, South Africa. *South Africa Journal of Geology* 97 (1):62-77.

Keifer, W.S. 2003. Impact Craters in the Solar System, Space Science Reference Guide, Second Edition, Lunar and Planetary Institute, NASA.

Shoemaker, E.M. 1974. Barringer Meteorite Crater, Coconino County, Arizona. In *Guidebook to the Geology of Barringer Meteorite Crater, Arizona*. Shoemaker, E.M. and S.W. Kieffer (editors) Publication no. 17, Reprinted 1988, Center for Meteorite Studies, Arizona State University, Tempe, Arizona: 1-11.

Thaisen, K. G., J. W. Head, L. A. Taylor, G. Y. Kramer, P. Isaacson, J. Nettles, N. Petro, and C. M. Pieters 2011.Geology of the Moscoviense Basin, *Journal of Geophysical Research,* 116, E00G07.